Annu. Rev. Nucl. Part. Sci. 1997. 47:395–428

RELATIVISTIC QCD VIEW OF THE DEUTERON

C. E. Carlson
Department of Physics, College of William and Mary, Williamsburg, Virginia 23187

J. R. Hiller
Department of Physics, University of Minnesota, Duluth, Minnesota 55812

R. J. Holt
Department of Physics, University of Illinois, Urbana-Champaign, Illinois 61801

KEY WORDS: electron scattering, form factors, photodisintegration, tensor polarization, hadron helicity conservation

ABSTRACT

The length scales for QCD and for nuclear physics are about the same, both about 1 fermi, and this directly motivates a search for a QCD explanation of nuclear phenomena, beginning with the deuteron. We first review the theoretical tools and results relevant to nuclear QCD, and then discuss data for several reactions. In particular, the remarkable data on deuteron photodisintegration agree with the naive perturbative QCD predictions for their scaling behavior and disagree with predictions from traditional approaches. This may be the first distinctive signature wherein considering the quark substructure in a nucleus is crucial in explaining some phenomenon.

CONTENTS

0163-8998/97/1201-0395$08.00

1. INTRODUCTION

Quantum Chromodynamics (QCD) (1) provides the most viable theory of the strong interactions. Almost all of the successes of this theory have been in the high-energy regime, where its quarks and gluons give a basis for parton analyses. This success follows from the relative ease of calculation for weakly coupled processes, where asymptotic freedom (2) admits perturbative methods.

Perturbation theory remains the primary mode for application of QCD. Nevertheless, consideration of exclusive processes (3), with use of factorization between weakly and strongly coupled contributions (4), has brought perturbative QCD (pQCD) to the realm of nuclear physics. It can now be used to investigate many aspects of nucleons and nuclei, and, as the simplest of nuclei, the deuteron has been a natural candidate for study. Here we will review many of the applications of QCD and of ideas based on QCD. Other reviews of applications to nuclear processes can be found in several conference proceedings (5–9) and other reviews (10, 11).

In principle, of course, QCD cannot be the theory of strong interactions unless all of nuclear physics can be understood in terms of quarks and gluons. The characteristic length scale of QCD (the size of a nucleon) is of the same order as the scale of nuclear systems. Thus, even if phenomena seem explainable by the traditional nuclear physics of mesons and nucleons, an alternative explanation in terms of quarks and gluons must eventually be found. This is a tall order, one that requires difficult nonperturbative calculations before it is filled.

This review does not address nonperturbative calculations in QCD. Such work is in its infancy. Instead, nonperturbative aspects will remain hidden in model wave functions or unspecified state vectors. We will focus on how pQCD can be used and what it can be persuaded to say about the deuteron.

As a quantum field theory, QCD is necessarily relativistic. We will use relativistic kinematics throughout. The most natural formulation is in terms of light-front (or light-cone) coordinates pioneered by Dirac (12, 13). The time coordinate, along which a system evolves, is taken to be $t + z$, where t is the ordinary time and z is a Cartesian coordinate. (We take $c = 1$.) This coordinate choice brings many advantages, including a well-defined Fock-state expansion

and separation of internal from total momentum. It has been very useful in perturbative calculations and is hoped to be the means by which nonperturbative QCD can make contact with the constituent quark model (14).

The individual quarks and gluons of QCD are not observed directly. They, and any other state with nonzero color charge, are confined inside color-singlet (color-neutral) states. Any attempt to separate color charges requires enough energy to produce additional particles that maintain neutrality on scales above the nucleon size. For ordinary mesons and baryons, this dictates unique valence states: a quark-antiquark pair for mesons, and three quarks for baryons. The six quarks of the deuteron admit a more complicated situation. In addition to the neutron-proton and delta-delta states, with two three-quark color singlets, there can be contributions from six-quark color singlets, the hidden color states (15). The evolution equations of pQCD imply that the latter configurations become dominant as small quark separations are approached (16, 17).

One of the earliest applications of pQCD to the deuteron was in the analysis of elastic scattering. Even before QCD, dimensional counting rules (18) were used to predict a $1/Q^{10}$ falloff for the dominant form factor F_d as a function of momentum transfer Q^2. The use of pQCD substantiates this conclusion, and predicts logarithmic corrections (19). Nonperturbative corrections have been included by invoking reduced amplitude analysis (20), in which experimentally determined nucleonic form factors F_N are used to describe the structure of the neutron and proton, and a reduced form factor (20) $f_d(Q^2) \equiv F_d(Q^2)/F_N^2(Q^2/4)$ is directly related to the probability for the two-nucleon system to remain intact. The argument of F_N is $Q^2/4$ because the deuteron is weakly bound and thus each nucleon must absorb half of the momentum transfer. The asymptotic behavior of f_d is $1/Q^2$. The available data (21, 22) are compared to this prediction in Figure 2.

As a spin-1 object, the deuteron has three elastic form factors (23). Each can be computed from matrix elements of the current operator between helicity states. Helicity rules derived from pQCD (24) can then be used (25) to analyze the relative strengths of the matrix elements and of the three form factors (26, 27). The combinations of matrix elements that appear include a kinematic factor $\eta \equiv Q^2/4M_d^2$. The characteristic mass scale of QCD, $\Lambda_{\rm QCD}$, also enters. To leading order in $\Lambda_{\rm QCD}/M_d$, the helicity- zero to helicity-zero matrix element is the only matrix element that matters when $Q^2 \gg 2M_d\Lambda_{\rm QCD}$ (27). Corrections to the next order in $\Lambda_{\rm QCD}/M_d$ have been computed (28). The crucial point is that $\eta \gg 1$ appears not necessary for the application of pQCD (27). However, such large momentum transfers are needed if the tensor polarization or tensor analyzing power, which is computed from ratios of form factors, is to approach the extreme asymptotic result of $-\sqrt{2}$ (29). Comparison with data (30) indicates that even the medium Q^2 regime has not yet been reached.

In models that do not preserve rotational covariance, one can encounter inconsistent results for the form factors. This happens because ordinarily the form factors are overdetermined by the helicity-matrix elements; breaking the symmetry destroys cancellations — the "angular condition" (31–33) — necessary for the overdetermined system to yield consistent results. One way to represent the extra freedom in the matrix elements is to introduce additional (unphysical) form factors (34, 35). Models can then be compared in terms of contributions from these additional form factors (34).

The pQCD and reduced amplitude analyses (36) can be extended to photodisintegration and other inelastic processes. They predict power-law falloffs for cross sections. For photodisintegration at 90°, pQCD has been particularly successful. At other angles, higher photon energies are needed to reach the same large momentum transfer to both nucleons.

In a relativistic formulation a spin-1 object can have a nonzero quadrupole moment with only an S-wave contribution (27). This is a consequence of spin-related boost effects that survive the zero-Q^2 limit (37). For the deuteron, the magnitude of this contribution is much smaller than the actual moment. Thus a D-wave contribution is necessary; however, a complete calculation needs to include the S-wave piece.

The contents of the remaining sections can be summarized as follows: Section 2 provides the necessary theoretical background, including a brief introduction to QCD and a description of light-front coordinates. Form factors for elastic scattering of the deuteron are discussed in Section 3. Dimensional counting and pQCD predictions are presented, and compared with currently available data for form factors and the tensor polarization. Section 4 is devoted to inelastic processes, such as photodisintegration, electrodisintegration, and $\overline{p}$ annihilation. Dimensional scaling analysis is applied to recent photodisintegration data. The dipole and quadrupole moments of the deuteron are analyzed in Section 5. Much of this discussion is applicable to spin-1 composites in general.

2. THEORETICAL BACKGROUND

2.1 *Quantum Chromodynamics*

The fundamental theory of the strong interactions is Quantum Chromodynamics (1). It is a quantum field theory for which the Lagrangian density is specified by

$$\mathcal{L} = -\frac{1}{2}\mathrm{Tr}(F^{\mu\nu}F_{\mu\nu}) + \bar{\psi}(i\not{D} - m)\psi \qquad 1.$$

where

$$F^{\mu\nu} = \partial^\mu A^\nu - \partial^\nu A^\mu + ig[A^\mu, A^\nu], \qquad 2.$$

$$iD^{\mu} = i\gamma^{\mu} - gA^{\mu}\,, \qquad 3.$$

and the gluon fields A^{μ} are traceless 3×3 matrices in the adjoint representation of SU(3). Here 3 is the number of colors for the quark field ψ, and color indices are suppressed.

The two critical properties of QCD that make possible predictions for exclusive reactions with large momentum transfer are asymptotic freedom (2) and factorization of hard and soft contributions (4). Asymptotic freedom means that the coupling is weak for the hard scattering contributions, and that these pieces can be computed perturbatively. Factorization leads to the following form for the amplitude of an exclusive process $AB \to CD$ (4):

$$T_{AB\to CD} = \int_0^1 \prod dx_i \phi_D^{\dagger}(x_i, Q)\phi_C^{\dagger}(x_i, Q) \times T_H \phi_B(x_i, Q)\phi_A(x_i, Q)\,, \qquad 4.$$

with Q the momentum transfer, assumed large, and each ϕ a distribution amplitude for the constituent quarks collinear up to the transverse scale Q. The quark scattering amplitude T_H takes quarks, collinear with their respective hadron, to collinear quarks. It is computed perturbatively. The distribution amplitudes are process independent. They represent the probability amplitudes for finding the hadrons in their valence quark states and are related to wave functions by integration over transverse momenta up to the scale Q. Their Q^2 dependence can be determined from evolution equations and renormalization group equations. Corrections to factorization are suppressed by powers of $1/Q$.

QCD is essential for the complete analysis of nuclear processes. Compared to QCD, standard nuclear theory is deficient in the following respects: Mesons and nucleons are only approximate degrees of freedom, the correct power-law falloff of form factors is not naturally reproduced (38), and nucleon-antinucleon terms present in intermediate states are not properly suppressed.

2.2 *Light-Front Formalism*

Light-front coordinates (12, 13, 39, 40) are defined by

$$x^{\pm} = t \pm z\,, \quad \mathbf{x}_{\perp} = (x, y)\,, \qquad 5.$$

and by the choice of x^+ as the time variable. Momentum components are similarly defined

$$p^{\pm} = E \pm p_z\,, \quad \mathbf{p}_{\perp} = (p_x, p_y)\,, \quad \underline{p} = (p^+, \mathbf{p}_{\perp})\,. \qquad 6.$$

Dot products are written

$$p\,x = Et - \mathbf{p}\cdot\mathbf{x} = \frac{1}{2}(p^+x^- + p^-x^+) - \mathbf{p}_{\perp}\cdot\mathbf{x}_{\perp}\,. \qquad 7.$$

Thus p^- is conjugate to x^+ and plays the role of energy; it is frequently called the light-cone energy. Particles remain on their mass shells ($m^2 = p^+p^- - p_\perp^2$) but intermediate states are off the light-cone energy shell ($p^-_{\text{total}} \neq \sum_i p_i^-$).

There are several reasons for the usefulness of the light-front formulation of QCD in the study of the deuteron. They include (7):

- a covariant many-body description with close connection to the nonrelativistic form and with separation of the dependence on relative and total momentum;
- predictions of leading powers for amplitudes;
- inclusion of "hidden color" states;
- kinematical boosts that simplify the extraction of form factors from current matrix elements;
- correct factorization of nuclear form factors and the reduced amplitude approach;
- covariant kinematics and the correct treatment of moments.

The alternative approach of an equal-time formulation suffers from difficulties with the complex vacuum state and interaction-dependent boosts. Also, a Fock-state expansion at equal time does not lead to a clear constituent picture; disconnected vacuum pieces contribute to every state. The covariant Bethe-Salpeter equation is also problematic, because it requires an infinite number of irreducible kernels in order to include the effects of channels with more than two valence particles.

In momentum space, the total momentum of a state can be separated from internal momentum variables. The internal variables are taken to be the longitudinal momentum fraction $x_i \equiv p_i^+/p^+_{\text{total}}$ and the relative transverse momentum $\mathbf{k}_{\perp i} = \mathbf{p}_{\perp i} - x_i \mathbf{p}_{\perp\text{total}}$.

These are the natural variables for a wave function that describes a state with a fixed number of particles. Such functions appear as the coefficients in an expansion of a state vector Ψ

$$\Psi = \sum_n \int [dx]_n \left[d^2k_\perp\right]_n \psi_n(x, \mathbf{k}_\perp) \left| n : x_i\, p^+_{\text{total}}, x_i \mathbf{p}_{\perp\text{total}} + \mathbf{k}_{\perp i} \right\rangle \qquad 8.$$

in terms of Fock states $|n : p_i^+, \mathbf{p}_{\perp i}\rangle$. Here quantum numbers other than momentum values are suppressed and

$$[dx]_n = 4\pi\delta\left(1 - \sum_{i=1}^n x_i\right) \prod_{i=1}^n \frac{dx_i}{4\pi\sqrt{x_i}}, \qquad 9.$$

$$\left[d^2k_\perp\right]_n = 4\pi^2\delta\left(\sum_{i=1}^{n}\mathbf{k}_{\perp i}\right)\prod_{i=1}^{n}\frac{d^2k_{\perp i}}{4\pi^2}\,. \qquad 10.$$

By construction, Ψ is an eigenstate of the total momentum. The requirement that it also be an eigenstate of light-cone energy determines the wave functions. This requirement is usually expressed as a field-theoretic Schrödinger equation

$$H_{\rm LC}\Psi = M^2\Psi\,, \qquad 11.$$

where $H_{\rm LC} = \mathcal{P}^+\mathcal{P}^- - \mathcal{P}_\perp^2$, M is the mass of the state, $\mathcal{P}^+$ and $\mathcal{P}_\perp$ are momentum operators, and $\mathcal{P}^-$ the light-cone energy operator. The equation can be reduced to a coupled set of integral equations for the wave functions. However, the complete nonperturbative formulation of this problem requires a better understanding of renormalization and other issues than is presently available (41). Fortunately, such a complete formulation is not necessary to make progress in understanding the deuteron from the point of view of QCD.

2.3 *Light-Front and Equal-Time Wave Functions*

A priori, there is not a simple connection between equal-time and light-front wave functions. One is defined at some fixed time t, the other at some fixed $x^+ = t + z$, i.e. at a different time for each different z. To turn one wave function into the other, one should know the time dependence, which means knowing the solution to the equations of motion.

However, there is a simple operational connection between equal-time and light-front wave functions (40). The idea is to find a mapping between the variables of (and possible factors multiplying) the wave functions that will turn a normalized solution of the equation of motion in one case into a normalized solution of the different-looking equation of motion for the other case. This will allow us to convert an equal-time wave function, and all the labor behind it, into a usable light-front wave function.

The equal-time formalism conserves three momentum but not energy, and the wave function depends on the three momentum $\vec{k}$. It satisfies, using the nonrelativistic case for illustration,

$$\int d^3k\,|\psi_{ET}(k_z, k_\perp)|^2 = 1 \qquad 12.$$

and

$$\left(E_{NR} - \frac{\vec{k}^2}{m_N}\right)\psi_{ET}(\vec{k}) = \int V_{ET}(\vec{k}, \vec{k}')\;\psi_{ET}(\vec{k}')\;d^3k', \qquad 13.$$

where, neglecting the binding energy, $E_{NR} = 0$.

The light-front formalism conserves the momentum components p^+ and $p_\perp$, and the wave function depends on the light-cone momentum fraction α and the transverse momenta. We convert from equal-time to light-front momenta by leaving the transverse momenta unchanged, $p_\perp = k_\perp$, and letting

$$\alpha \equiv \frac{E_k + k_z}{E_k}. \qquad 14.$$

where $E_k \equiv \sqrt{m_N^2 + \vec{k}^2}$. This defines k_z given α or vice versa, and leads to a Jacobian

$$d^3k = \frac{E_k}{\alpha(2-\alpha)} d\alpha\, d^2p_\perp. \qquad 15.$$

Now obtain the light-cone wave function and potential from

$$\psi_{LF}(\alpha, p_\perp) = \left(\frac{E_k}{\alpha(2-\alpha)}\right)^{\frac{1}{2}} \psi_{ET}(k_z, k_\perp) \qquad 16.$$

and

$$V_{LF}(\alpha, p_\perp; \alpha', p'_\perp) = \left(\frac{E_k}{\alpha(2-\alpha)}\right)^{\frac{1}{2}} V_{ET}(\vec{k}, \vec{k}') \left(\frac{E_{k'}}{\alpha'(2-\alpha')}\right)^{\frac{1}{2}}. \qquad 17.$$

One can easily show that this wave function satisfies

$$\int d\alpha\, d^2p_\perp\, |\psi_{LF}(\alpha, p_\perp)|^2 = 1 \qquad 18.$$

and the light-front version of the Schrödinger equation

$$\frac{1}{2}\left(m_d - \frac{m_N^2 + p_\perp^2}{\alpha(2-\alpha)m_N}\right)\psi_{LF}(\alpha, p_\perp) = \int V_{LF}(\alpha, p_\perp; \alpha', p'_\perp)\, \psi_{LF}(\alpha', p'_\perp)\, d\alpha'\, d^2p'_\perp. \qquad 19.$$

It is wave functions made kinematically relativistic in this fashion, or fashions like this, that are used to calculate, for example, the spectrum of relativistic spectator nucleons in works such as References 42, 43, and 44.

3. FORM FACTORS

The standard Rosenbluth cross section (45) for elastic electron scattering is

$$\frac{d\sigma}{d\Omega} = \frac{\alpha^2 \cos^2(\theta/2)}{4E^2 \sin^4(\theta/2)} \frac{E'}{E}[A(Q^2) + B(Q^2)\tan^2(\theta/2)]. \qquad 20.$$

For a spin-1 particle, the generic form factors A and B are given by

$$A = G_C^2 + \frac{2}{3}\eta G_M^2 + \frac{8}{9}\eta^2 G_Q^2,$$
$$B = \frac{4}{3}\eta(1+\eta)G_M^2\,, \qquad 21.$$

where $\eta = \frac{Q^2}{4M^2}$ is a kinematic factor. The charge, magnetic, and quadrupole form factors, G_C, G_M, and G_Q, respectively, are extracted from matrix elements

$$G^{\mu}_{h'h} = \langle p'h'|J^{\mu}|ph\rangle\,, \qquad 22.$$

of the electromagnetic current J^{μ}. Here $|ph\rangle$ is an eigenstate of momentum p and helicity h. Assuming parity and time-reversal invariance, this matrix element can be written in the form (23)

$$G^{\mu}_{h'h} = -\big\{G_1(Q^2)\epsilon'^{*}\cdot\epsilon[p^{\mu}+p'^{\mu}] + G_2(Q^2)[\epsilon^{\mu}\epsilon'^{*}\cdot q - \epsilon'^{*\mu}\epsilon\cdot q]$$
$$- G_3(Q^2)\epsilon\cdot q\,\epsilon'^{*}\cdot q(p^{\mu}+p'^{\mu})/(2M^2)\big\}, \qquad 23.$$

with $Q^2 = -q^2$, $q = p' - p$, and $\epsilon \equiv \epsilon_h$ and $\epsilon' \equiv \epsilon_{h'}$ the initial and final polarization vectors of the deuteron. The charge, magnetic, and quadrupole form factors are determined by the $G_i(Q^2)$ (23)

$$G_C = G_1 + \frac{2}{3}\eta G_Q, \quad G_M = G_2, \quad G_Q = G_1 - G_2 + (1+\eta)G_3\,. \qquad 24.$$

Each of these form factors can be obtained from the plus component of three matrix elements (46, 25) in the standard light-cone frame (47) $q^+ = 0$, $q_y = 0$, $q_x = Q$:

$$G_C = \frac{1}{2p^+(2\eta+1)}\left[\frac{16}{3}\eta\frac{G^+_{+0}}{\sqrt{2\eta}} - \frac{2\eta-3}{3}G^+_{00} + \frac{2}{3}(2\eta-1)G^+_{+-}\right],$$
$$G_M = \frac{2}{2p^+(2\eta+1)}\left[(2\eta-1)\frac{G^+_{+0}}{\sqrt{2\eta}} + G^+_{00} - G^+_{+-}\right], \qquad 25.$$
$$G_Q = \frac{1}{2p^+(2\eta+1)}\left[2\frac{G^+_{+0}}{\sqrt{2\eta}} - G^+_{00} - \frac{\eta+1}{\eta}G^+_{+-}\right].$$

3.1 *Predictions at High Q^2*

COUNTING RULES According to dimensional counting rules (18), the cross section for a process has the asymptotic behavior

$$\frac{d\sigma}{dt} \sim \frac{f(t/s)}{s^{n-2}}\,, \qquad 26.$$

where n is the number of ingoing and outgoing elementary fields involved. This behavior is derivable from the underlying theory if the theory has scale-invariant tree graphs, only soft corrections from loops, and strong suppression of pinch singularities. QCD has these properties.

The original derivation (18) begins with the observation that the Feynman amplitude M_n for n constituent fields has dimension of energy to the $4-n$, assuming that the individual particle states have the normalization $\langle p'|p\rangle = 2E\delta^3(\vec{p}\,' - \vec{p})$. At large energy and momentum transfer, it is assumed that constituent masses and binding energies can be ignored, and the center of mass energy $\sqrt{s}$ is the only energy scale available. We then have

$$M_n \sim \frac{f_n(t/s)}{(\sqrt{s})^{n-4}}\,. \qquad 27.$$

The amplitude M for scattering of physical hadrons is obtained by integrating over momenta of constituents for each hadron. Assume that the primary contribution to each integral comes from the region where all constituents have a finite fraction of the hadron momentum. The hadron amplitude M will then have the same behavior as the constituent amplitude M_n. Because the cross section is related to the amplitude by $d\sigma/dt \sim |M|^2/s^2$, Equation 26 is obtained.

When this rule is applied to elastic electron-hadron scattering, the asymptotic behavior of the dominant form factor $\sqrt{A}$ is shown to be (18)

$$F(Q^2) \sim \left(\frac{1}{Q^2}\right)^{n-1}, \qquad 28.$$

with n the number of constituents of the hadron and Q^2 the magnitude of the momentum transferred to the hadron. For the deuteron, $n = 6$ and $F \sim 1/Q^{10}$. Because each constituent of the deuteron experiences a momentum transfer of only $Q^2/36$, Q^2 must be quite large. When $Q^2/36$ is small, the reduced amplitude approach (20) must be used; this approach is discussed in a later subsection.

PERTURBATIVE QCD The counting rules can be derived from QCD by applying the factorized expression (4). The leading perturbative contribution to the hard scattering amplitude T_H then determines the s dependence of the hadronic amplitude. Factorization requires that one be able to neglect the transverse momentum of the quarks compared to the transverse momentum flowing through the hard scattering of collinear quarks.

In QCD, the counting rules are modified by logs from loops. These corrections are mild because of asymptotic freedom. Endpoint contributions, where spectators have longitudinal momenta near zero, are suppressed by Sudakov form factors associated with gluonic radiative corrections (8).

Hadronic helicity is conserved to leading order in m_q/Q because helicity is conserved for massless quarks coupled to vector gluons, and the hadron helicity is the sum of the quark helicities (24). To leading order the constituents are in $L_z = 0$ states. Thus there is no orbital contribution.

A direct computation of the perturbative QCD (pQCD) prediction for the helicity-zero to helicity-zero deuteron form factor has been done by Farrar et al (48). The computation obtains the amplitude T_H for the scattering of six collinear quarks to a new state of six collinear quarks. There are $\sim 20 \cdot 10^6$ diagrams that connect the six quarks with five gluons. The number of gluons is the minimum necessary to transfer momentum to all quarks, and thereby keep them collinear with their respective hadron. The quark amplitude is then combined with distribution amplitudes to compute the form factor. There is some concern over the correct momentum scale to be used in determining the strong coupling used in T_H.

Helicity and angular momentum conservation force many diagrams to be zero for collinear quarks. There is also a large amount of cancellation between nonzero diagrams.

The distribution amplitudes were chosen in a weak binding limit, where each nucleon has one half of the deuteron momentum. This neglects non-nucleonic components, such as hidden color states. Nucleon distribution amplitudes were constructed in the nonrelativistic limit (3) where

$$\phi_N(x, Q^2) = \int_0^Q \frac{d^2k_\perp}{16\pi^3}\psi(\mathbf{k}_\perp, k_3 = Mx - m)\,. \qquad 29.$$

For the weak binding condition, we have $M \simeq 2m_N$ and $x \simeq 1/2$. The nucleon distribution amplitudes were checked by computing the nucleon form factors. The sensitivity to the choice of distribution amplitude is not large.

The result for the form factor (48) is almost four orders of magnitude smaller than experiment at $Q^2 \simeq 4\,\mathrm{GeV}^2$. Thus if pQCD is to be applicable at this momentum scale, additional considerations must be taken into account. As discussed below in the subsection on hidden color, non-nucleonic contributions become important at large momentum transfers (49). Also, the poor convergence of perturbation theory can mean that the lowest-order prediction is incorrect in normalization by factors of two or more (3). In addition, the couplings used in T_H need to be selected with care. Brodsky suggests (5) that these couplings be defined relative to the heavy quark potential and evaluated at the momenta of the exchanged gluons.

SPIN-DEPENDENT RESULTS The counting rules give correctly the Q^2 dependence of the leading amplitude. For the deuteron, there are three independent amplitudes, and we would like to find the Q^2 dependence of each of them.

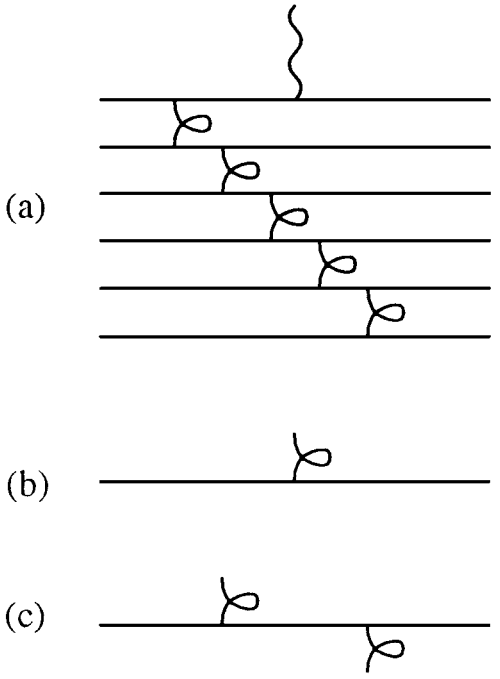

Figure 1 (*a*) One lowest-order diagram for elastic *ed* scattering at high momentum transfer; (*b*) and (*c*) are subgraphs of (*a*). The lines with a single corkscrew represent gluons, and the wiggly line is a photon.

To do so, we just need a few rules to tell us how much it costs to arrange the helicities in different ways than in the largest amplitude.

It is convenient to think in the Breit frame (where the initial and final deuteron three momenta are equal in magnitude but opposite in direction), and use the helicity amplitudes $G^I_{\lambda,\lambda'}$. (The superscript here is the helicity of the virtual photon, and the subscripts are the helicities of the incoming and outgoing deuterons.) In the Breit frame, angular momentum conservation dictates that many of the amplitudes be zero: We must have $\lambda' = I - \lambda$. A typical lowest-order diagram is shown in Figure 1*a*. Here are three rules (25).

The one-gluon rule: Where only one gluon connects to a quark (Figure 1*b*), the largest amplitude has a transverse (T) gluon and quark helicity is conserved. If the gluon is longitudinal (L), the quark helicity must flip and the amplitude is smaller by a factor of $O(m/Q)$, where m is some mass scale. The two-gluon (or gluon-photon) rule: If one gluon is absorbed and one is emitted (Figure 1*c*), the largest amplitude has one transverse gluon and one longitudinal gluon, and

quark helicity is conserved. If both gluons are longitudinal the amplitude is reduced by $O(m/Q)$ and quark helicity is flipped. If both gluons are transverse, the amplitude is zero. The transverse-gluon rule: Two quark lines connected by a transverse gluon have opposite helicity.

There are also rules that are relevant when more than two gluons connect to a given quark line and when triple or quadruple gluon interactions are involved, but they give the same results as diagrams that can be analyzed using only the above rules.

The leading amplitude is G^0_{00}. It can be arranged so that gluon polarization and quark helicity alternate is just the right way to allow a maximum amplitude for every piece of the diagram. Amplitude G^+_{+0} is next, suppressed by a factor of $O(m/Q)$ because one quark helicity flip is required, and G^0_{+-} is suppressed by $O(m^2/Q^2)$ because two quark helicity flips are required. In terms of the more common charge, magnetic, and quadrupole form factors (conversions are given below when we discuss higher corrections), one has G_C falling like Q^{-10}, and both G_M and G_Q falling like Q^{-12}, with

$$\lim_{Q^2\to\infty} G_C = \frac{Q^2}{6m_d^2} G_Q. \qquad 30.$$

These results have interesting and testable consequences for the tensor polarization T_{20}, also discussed below. Another interesting and important question is how large the next-to-leading power-law corrections are. The Breit frame is good for thinking about the leading powers for each form factor, as was done in Reference 25, but one notices, for example, that in transforming helicity amplitudes to the $q^+ = 0$ light-front frame, the leading terms for each form factor are indeed invariant, but the next-to-leading corrections are of order m_d^2/Q^2, which are hardly small. Corrections should be estimated in the $q^+ = 0$ light-front frame, as was done in Reference 27 and is discussed below, because there the only vertex that enters is the $d \to 6q$ one; in other frames there are for example $\bar{q} + d \to 5q$ diagrams whose size is not known relative to the other.

REDUCED FORM FACTORS In the rest frame the relativistic deuteron wave function factorizes in the zero binding limit and can be written as (50)

$$\psi_d = \psi_d^{\text{body}} \times \psi_N \times \psi_N \,. \qquad 31.$$

This no longer holds when the deuteron is boosted to a state with momentum much larger than the scale of the internal transverse nucleon momentum. However, for large momentum transfer, the boosted wave function can be related to the factorized form in the rest frame via a hard scattering process. This leads

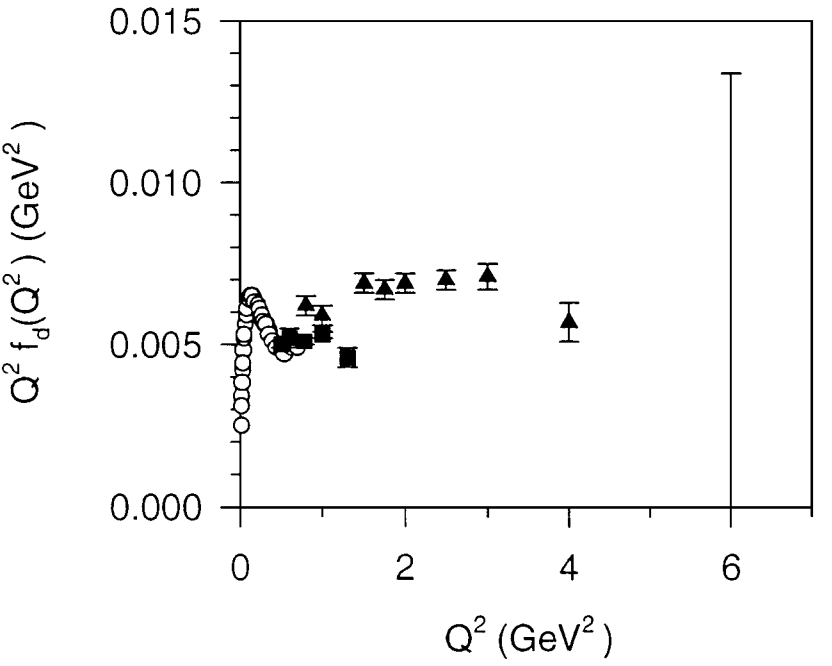

Figure 2 The behavior of f_d, the reduced form factor, computed from Equation 32 of the text and data for $\sqrt{A}$ (21, 22). The open circles are from Platchkov et al, the squares from Cramer et al, and the triangles from Arnold et al.

directly to the notion of the reduced form factor (20)

$$f_d(Q^2) \equiv \frac{F_d(Q^2)}{F_{1n}(Q^2/4)F_{1p}(Q^2/4)}\,. \qquad 32.$$

Hadron helicity conservation implies that this is the form for the helicity-zero to helicity-zero form factor. This form, compared with data, is shown in Figure 2.

From dimensional counting one obtains $f_d(Q^2) \sim 1/Q^2$. In pQCD there are computable logarithmic corrections associated with the running coupling and the Q^2 evolution of the deuteron distribution amplitude. Including these corrections yields (19)

$$f_d(Q^2) \sim \frac{\alpha_s(Q^2)}{Q^2}\left(\ln\frac{Q^2}{\Lambda_{\rm QCD}}\right)^{-2C_F/5\beta}\,, \qquad 33.$$

where $2C_F/5\beta = -8/145$ for two flavors of quarks.

At large Q^2, QCD is not consistent (50) with the traditional decomposition (51) of the generic form factor

$$F_d(Q^2) = F_N(Q^2) \times F_{\text{body}}(Q^2)\,. \qquad 34.$$

At small momentum transfer, the Fermi motion of the nucleon is sufficient to keep the struck nucleon nearly on shell, but for large momentum transfer, the struck nucleon goes off shell and off-shell nuclear form factors are needed. The size of the momentum transfer is measured relative to $2M_d\epsilon_d \simeq 100\,\text{MeV}$, where ϵ_d is the deuteron binding energy. For small Q^2, F_d is nearly equal to 1, which limits the usefulness of Equation 34.

3.2 *Six-Quark Clusters*

When the constituents of the nucleus are far apart, a description in terms of neutrons and protons is accurate. The question is what happens to the material inside the nucleus when the pieces come close to each other. One view is that the pieces never come close to each other. A repulsive force keeps them apart. One may also suppose that even if the nucleons are pushed close together they maintain their nucleonic character and behave as recognizable neutrons and protons. This viewpoint we shall refer to as the two-nucleon, or 2*N*, model for the behavior of nuclear material at short interparticle distances. (Note that it is not possible to take a neutron — three quarks in an S-state with the correct spin, isospin, and color — and precisely overlap it with a proton. The Pauli principle at the quark level prevents it.)

An alternative viewpoint is that if two nucleons come sufficiently close together, the quarks within them reorganize or mix into a new state where each quark is in the lowest-energy spatial state, and the color-spin-flavor part of the quark wave function is uniquely fixed by the requirement that it be a totally antisymmetric colorless state of the desired spin and isospin. The six quarks may thus lie on top of each other. This model of a quark cluster is also an extreme viewpoint, and we refer to it as a six-quark, or 6-*q*, model. Kisslinger and co-workers (52) have developed a phenomenological approach to this mixing.

When the six-quark state was first written down (15), it led to the idea of "hidden color." The 6-*q* state is a color singlet overall, but if one selects three definite quarks, those quarks do not generally form a color singlet. For a 6-*q* state that has the quantum numbers of the deuteron, a given set of three quarks has a 20% chance of being a color singlet, divided as 9% probability of having the quantum numbers of a nucleon and 11% probability of having those of the delta resonance. The remainder of the state can be written out as a collection of terms, 80% by probability, which have three quarks in a color octet coupled to another three quarks in a color octet (16). This part of the state

was referred to as hidden color. At short distances, the deuteron state evolves (49) into this combination of possibilities with 80% hidden color. From this one can conclude that the nucleon-nucleon potential will appear repulsive at short distances, because work must be done to convert $2N$ to hidden color states as the nucleons are brought closer together (17).

There is an alternative expression of the state that leads to a different vision of its nature (53). One may write the state as a sum of product wave functions in which the quarks are always grouped into colorless quark triplets. For example, the first term consists of quarks 1, 2, and 3 in a color singlet with the quantum numbers of a nucleon with quarks 4, 5, and 6 also in a color singlet with the quantum numbers of a nucleon. The second term is similarly two factors, but now involving different quarks, say quarks 1, 2, and 4 in a color singlet with the quantum numbers of the nucleon and quarks 3, 5, and 6 in a similar state, and so on. There is no hidden color. However, the state is not equivalent to a simple overlap of two nucleons. Additionally, the very same state could be expanded in terms of delta-like objects, wherein every term consists of two factors, each having three overall colorless quarks with the quantum numbers of the delta. Some lessons are clear: We have to be careful in searching for such states by looking for phenomena dependent upon the hidden color or upon the delta-like components in the state. Unfortunately, the power-law falloff associated with hidden color components is the same as that for nucleonic components; therefore, the power-law behavior cannot be used to detect hidden color.

It is well known that the nucleon-nucleon force is repulsive at short range. Clearly, the nucleon-nucleon scattering data, analyzed with the assumption that nucleons are the only degrees of freedom, leads to a repulsive nucleon-nucleon potential. This, however, is a single-channel analysis of a coupled-channel problem. The other channels possible include what we may describe as hidden-color channels, which disappear at long distances.

It is not difficult to devise a pedagogic coupled-channel model that has only attractive potentials and yet mocks the nucleon-nucleon situation of having an apparent repulsive potential when viewed only in terms of one long-distance channel (54). More realistically, Reference 55 provides a coupled-channel study of a nominally two-nucleon system, with $2N$ interacting by meson exchange at long distances and having a 6-q cluster at short distances. The NN wave function diminishes at short range — an apparent repulsion — but a 6-q core comes into being. In a deuteron, the quark cluster core is 1–2% by probability yet still has a notable effect on the form factors (15), or on the numbers of fast spectator protons in hadronic (42) or leptonic reaction (44).

Thus we learn that an apparently repulsive potential is not proof of an actual repulsion at short distances since we have a coupled-channel situation. One cannot argue that a repulsive potential prevents the nucleons from ever

coalescing into a six-quark cluster. Arguments about formation of a 6-q state have to be made on other grounds.

DISTINGUISHING A 6-q CLUSTER One prediction of the $2N$ model that can distinguish between it and a 6-q cluster is the factorization of the leptonic and hadronic variables that should follow in lepton-induced breakup of the deuteron with a backward (spectator) nucleon observed. If the backward nucleon is a proton, the process proceeds by having the neutron struck and the proton emerging with the Fermi momentum it had at the moment of reaction. For electron scattering, the cross section reads

$$\frac{d\sigma_{2N}}{dx\,dy\,d\alpha\,d^2p_T} = \frac{4\pi\alpha_{em}^2 m_N E}{Q^4} \times \left(1+(1-y)^2\right)(2-\alpha)F_{2n}(\xi)\cdot|\psi(\alpha,\,p_T)|^2\,, \qquad 35.$$

where α and p_T are hadronic variables, namely the light-front momentum fraction and transverse momentum variables for the outgoing proton as defined in Section 2.3, and x and y are lepton variables, namely $Q^2/2m_N\nu$ and the dimensionless lepton energy loss ν/E where ν is the actual lepton energy loss and E is the incoming lepton energy in the lab; ξ is the momentum fraction of the struck quark within the neutron, which can be shown to be $x/(2-\alpha)$.

If the outgoing proton variables are fixed, the x dependence should be dominated by the known neutron cross section. One can test this. Model calculations show a significant difference in x dependence if the 6-q models are relevant, as they may be when the backward proton momentum is large (56), so that we have a good signature for the success or failure of the $2N$ model independently of the intrinsic correctness of the NN wave function. An experiment to study backward proton momenta is approved at the Thomas Jefferson National Accelerator Facility (TJNAF) (57).

3.3 *Estimates of Q^2 Scales*

Hadron helicity conservation implies that the helicity-zero to helicity-zero matrix element G_{00}^{+} dominates at large momentum transfer (24). (We are back in the $q^+ = 0$ light-front frame, and the superscript is the component of the Lorentz vector, as in Equation 22.) Corrections to this are of order $\Lambda_{\rm QCD}/Q$ and Λ_{QCD}/M_d (27), where $\Lambda_{\rm QCD}$ is the typical QCD momentum scale, in the range of 100 to 200 MeV. Based on estimates by Carlson & Gross (25), the helicity-changing matrix elements are suppressed by one or two powers of $\Lambda_{\rm QCD}/Q$

$$G_{+0}^{+} \sim \frac{\Lambda_{\rm QCD}}{Q}G_{00}^{+}\,, \quad G_{+-}^{+} \sim \left(\frac{\Lambda_{\rm QCD}}{Q}\right)^2 G_{00}^{+}\,. \qquad 36.$$

The G_{00}^+ contributions then dominate G_C, G_M, and G_Q if $Q^2 \gg 2M_d\Lambda_{\rm QCD} \simeq 0.8\,{\rm GeV}^2$ or equivalently $\eta \gg \Lambda_{\rm QCD}/2M_d \simeq 0.05$ (27). This leads to the form factor ratios (27) $G_C : G_M : G_Q = (1 - \frac{2}{3}\eta) : 2 : -1$ and

$$\frac{B}{A} \simeq \frac{4\eta(\eta+1)}{\eta^2+\eta+3/4}\,. \qquad 37.$$

The ratio of G_C to G_Q was first obtained by Chung et al (46). A simple form that satisfies both the large Q^2 and zero Q^2 limits

$$G_C = \left(\frac{1}{Q_d} + \frac{Q^2}{6M_d^2}\right) G_Q\,, \qquad 38.$$

where Q_d is the quadrupole moment, has been suggested by Carlson (29).

Corrections of order $\Lambda_{\rm QCD}/M_d$ have been computed by Kobushkin & Syamtomov (28). They keep contributions from G_{+0}^+ by writing

$$G_{+0}^+ \simeq a\frac{\Lambda_{\rm QCD}}{Q} G_{00}^+\,, \qquad 39.$$

with the constant a determined by a fit to the zero in B. The value they obtain for a is near 5. The expressions for the form factors become

$$\begin{aligned} G_C &\simeq -\frac{1}{2p^+(2\eta+1)}\left[\frac{2\eta-3}{3} - \frac{4\sqrt{2}}{3}a\frac{\Lambda_{\rm QCD}}{M_d}\right] G_{00}^+ \\ G_M &\simeq \frac{2}{2p^+(2\eta+1)}\left[1 + \frac{a}{\sqrt{2}}\left(1-\frac{1}{2\eta}\right)\frac{\Lambda_{\rm QCD}}{M_d}\right] G_{00}^+ \qquad 40. \\ G_Q &\simeq -\frac{1}{2p^+(2\eta+1)}\left[1 + -\frac{a}{\sqrt{2\eta}}\frac{\Lambda_{\rm QCD}}{M_d}\right] G_{00}^+\,. \end{aligned}$$

There is then a finite contribution to the large-Q^2 ratios that involve G_M. Corrections of order $(\Lambda_{\rm QCD}/M_d)^2$ could also be considered.

3.4 *Rotational Covariance*

That there are only three form factors for the deuteron implies that there are constraints on the current matrix elements and that the expressions in Equation 25 are not unique. By demanding rotational covariance for these matrix elements one can show that the following angular condition must be satisfied (31–33) in the frame where $\mathbf{p}'_\perp = -\mathbf{p}_\perp = \frac{1}{2}\mathbf{q}_\perp$ and $p'^+ = p^+$:

$$(1+2\eta)G_{++}^+ + G_{+-}^+ - \sqrt{8\eta}G_{+0}^+ - G_{00}^+ = 0\,. \qquad 41.$$

In order that the matrix elements satisfy this constraint, the current operator must transform properly (33, 58) and the state vectors must be eigenstates of

total spin. Models may not have these properties, and the angular condition will not be met.

If the angular condition is not met, the results obtained for form factors will depend on the matrix elements used to compute them (32). A comparison of the consequences of various choices is given by Karmonov (34). The choices include the one made by Brodsky & Hiller (27), although their work was an investigation of asymptotic behavior rather than a model calculation. Ways to meet the constraint are studied in References 32 and 46. The consequences of model choices for the case of another spin-1 object, the ρ, have been studied by Keister (33) and Cardarelli et al (59).

A covariant formulation of light-front dynamics has been developed to help with these calculations (35, 60); it uses a vector ω to fix the choice of the light-front plane. This introduces additional terms in the tensor structure of the current matrix elements. A total of 11 form factors is then needed (35, 34)

$$\langle p'h'|J^\mu|ph\rangle = \tilde{G}^\mu_{h'h}(\omega) = G^\mu_{h'h} + \epsilon'^{\nu *} B^\mu_{\nu\sigma}(\omega)\epsilon^\sigma \,, \qquad 42.$$

where $G^\mu_{h'h}$ is given in (23) and

$$\begin{aligned} B^\mu_{\nu\sigma} = \frac{M_d^2}{2\omega\cdot p}\,\omega^\mu\Bigg[& B_1(Q^2) g_{\nu\sigma} + B_2(Q^2)\frac{q_\nu q_\sigma}{M_d^2} \\ & + B_3(Q^2) M_d^2 \frac{\omega_\nu\omega_\sigma}{(\omega\cdot p)^2} + B_4(Q^2)\frac{q_\nu\omega_\sigma - q_\sigma\omega_\nu}{2\omega\cdot p}\Bigg] \\ & + B_5(Q^2)(p'^\mu + p^\mu) M_d^2 \frac{\omega_\nu\omega_\sigma}{(\omega\cdot p)^2} \\ & + B_6(Q^2)(p'^\mu + p^\mu)\frac{q_\nu\omega_\sigma - q_\sigma\omega_\nu}{2\omega\cdot p} \\ & + B_7(Q^2) M_d^2 \frac{g^\mu_\nu\omega_\sigma + g^\mu_\sigma\omega_\nu}{\omega\cdot p} + B_8(Q^2) q^\mu \frac{q_\nu\omega_\sigma + q_\sigma\omega_\nu}{2\omega\cdot p}\,. \end{aligned} \qquad 43.$$

To eliminate the unphysical form factors, more matrix elements are used, including those of current components other than the plus component.

The angular condition (41) is consistent with the large-Q^2 behavior predicted by pQCD for the three physical form factors (33). It is in model calculations that the difficulties arise. In fact, the large-Q^2 limit of the form factors cannot be reproduced using one-body currents in a constituent quark model (33).

3.5 *Comparison with Experiment*

Electron-deuteron elastic scattering has been vigorously pursued experimentally during the past decade. The central problem in using electron elastic scattering to measure the structure of the deuteron is that only A and B are

measured if no polarization quantities are observed. Recently, tensor polarization (t_{20}) and analyzing power (T_{20}) measurements have been performed. The tensor analyzing power is defined by (61)

$$T_{20} = \frac{1}{\sqrt{2}} \frac{d\sigma_+ + d\sigma_- - 2d\sigma_0}{d\sigma_+ + d\sigma_- + d\sigma_0}, \qquad 44.$$

where $d\sigma_\lambda$ is the differential cross section for elastic scattering of an electron from a deuteron with polarization λ. In terms of the form factors, it can be written as

$$T_{20}(Q^2, \theta) = -\frac{\frac{8}{9}\eta^2 G_Q^2 + \frac{8}{3}\eta G_C G_Q + \frac{2}{3}\eta G_M^2 \left[\frac{1}{2} + (1+\eta)\tan^2\left(\frac{\theta}{2}\right)\right]}{\sqrt{2}\left[A + B\tan^2\left(\frac{\theta}{2}\right)\right]}. \qquad 45.$$

(Note that some early work defined T_{20} as the above without the G_M terms.) When $\eta \gg \Lambda_{\rm QCD}/M_d$ this reduces to (26–28)

$$T_{20}(\theta) \simeq -\sqrt{2}\frac{\eta\left[\eta - \frac{1}{2} + (\eta+1)\tan^2\frac{\theta}{2}\right]}{\eta^2 + \eta + \frac{3}{4} + 4\eta(\eta+1)\tan^2\frac{\theta}{2}}. \qquad 46.$$

In the very large Q^2 region, $\eta \gg 1$ and

$$T_{20} \simeq -\sqrt{2}\frac{1 + \tan^2\frac{\theta}{2}}{1 + 4\tan^2\frac{\theta}{2}}. \qquad 47.$$

When θ is zero, this becomes just $-\sqrt{2}$, which is the asymptotic value usually quoted (29, 62). For $\eta \ll 1$, Brodsky & Hiller (27) obtained an expression that is more relevant for experiment

$$T_{20} \simeq \frac{2\sqrt{2}}{3}\eta\left(1 - 2\tan^2\frac{\theta}{2}\right). \qquad 48.$$

Kobushkin & Syamtomov (28) include the $\Lambda_{\rm QCD}/M_d$ corrections.

The tensor polarizations were measured with recoil deuteron polarimeters while the tensor analyzing powers were measured with tensor polarized deuteron targets.

The pQCD predictions for B/A and T_{20} are compared with experiment (21, 30, 63) in Figures 3 and 4. For comparisons between pQCD and results computed from model nuclear wave functions, see Reference 26. Comparisons between data and the nuclear model results are given in References 46, 62, and 64. It is essential to extend these data to higher momentum transfers to test the theoretical calculations. New experiments (65) are planned at TJNAF to extend the momentum transfer range of $A(Q^2)$, $B(Q^2)$ and t_{20}.

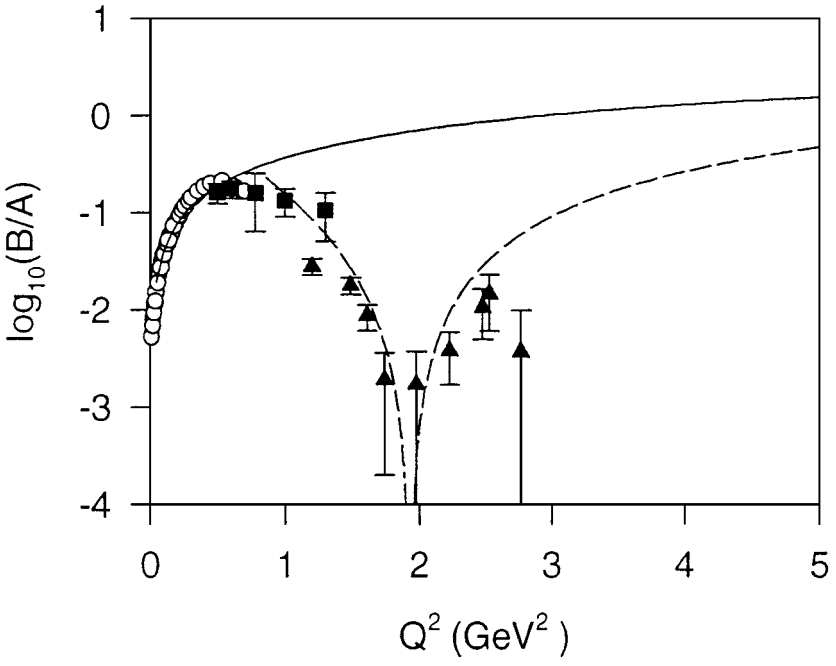

Figure 3 The form factor ratio B/A. The data (22, 63) are from Platchkov et al (*open circles*), Cramer et al (*squares*), and Bosted et al (*triangles*). In the case of Bosted et al, the values of $A(Q^2)$ were not given explicitly, but were extracted from tabulated cross-section data. The solid line is plotted from Equation 37 of the text; this is the ratio obtained by Brodsky & Hiller (27). The dashed line includes the correction of order $\Lambda_{\rm QCD}/M_d$ obtained by Kobushkin & Syamtomov (28).

4. PHOTODISINTEGRATION AND OTHER PROCESSES

4.1 *Theoretical Developments*

COUNTING RULES AND PQCD For photodisintegration, where the number of ingoing and outgoing fields is 13, the dimensional counting rule (26) becomes (18)

$$\left.\frac{d\sigma}{dt}\right|_{\gamma d\to np} \sim F(\theta_{cm})s^{-11}. \qquad 49.$$

Hadron helicity conservation (24) implies that the final nucleon helicities are related to the initial deuteron helicity by (36)

$$\lambda_d = \lambda_p + \lambda_n\,. \qquad 50.$$

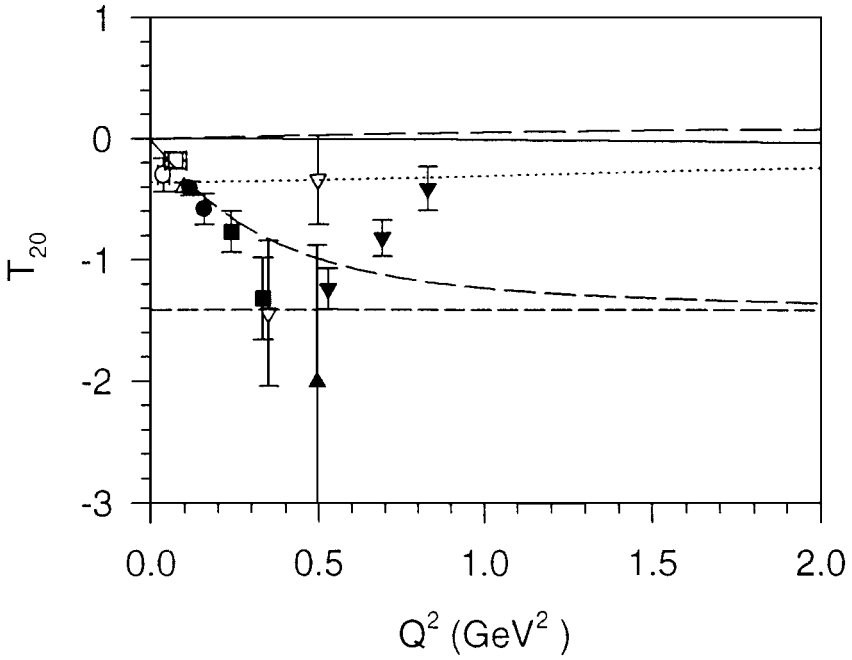

Figure 4 The tensor analyzing power T_{20}. The data (30) are from Schulze et al (*solid circles*), Dmitriev et al (*open circle*), Voitsekhovshii et al (*open square*), Gilman et al (*solid squares*), Boden et al (*solid up triangle*), Garcon et al (*solid down triangle*), Popov et al (*open down triangle*), and Ferro-Luzzi et al (*open up triangle*). The angles range from 10° to 80°. The theoretical curves are for 0° (*long dash*) and 70° (*solid*) from Brodsky & Hiller (27) and Equation 46 of the text, the correction of order $\Lambda_{\rm QCD}/M_d$ at 0° (*dotted*) by Kobushkin & Syamtomov (28), the model of Carlson (*medium dash*) (29), and the extreme asymptotic limit of $-\sqrt{2}$ (*short dash*).

REDUCED AMPLITUDE ANALYSIS It is generally believed that the constituent counting rules should only be valid at the highest energy, where pQCD is valid. The reduced nuclear amplitude analysis (RNA) was developed (20, 36) as a way of effectively taking into account many of the nonperturbative effects at intermediate energy. It incorporates covariance, QCD scaling laws, and gauge invariance, and is a generalization of the reduced-form-factor approach that was successfully applied (20) to electron-deuteron elastic scattering.

For any amplitude $\mathcal{M}$ involving A nucleons, a reduced amplitude m is defined by

$$m(s,t) = \mathcal{M}(s,t) \Big/ \prod_{i=1}^{A} F_N\left(\hat{t}_i = q_i^2\right), \qquad 51.$$

where q_i is the momentum transferred to the i^{th} nucleon in the zero-binding approximation. Dimensional counting and pQCD scaling rules imply that

$$m \sim f\left(\frac{\text{invariants}}{s}\right) \Big/ p_T^{n-4}, \qquad 52.$$

with $p_T^2 = tu/s$. To the count n of ingoing and outgoing fields, each reduced nucleon now contributes one, rather than three. For photodisintegration, we have $n = 5$ and

$$m \sim f(\theta_{cm})/p_T\,. \qquad 53.$$

The form of the reduced amplitude implies the following form for the differential cross section (36):

$$(d\sigma/d\Omega)_{cm} \sim \frac{1}{\sqrt{s(s-M_d^2)}} F_p^2(\hat{t}_p) F_n^2(\hat{t}_n) \frac{1}{p_T^2} f^2(\theta_{cm})\,. \qquad 54.$$

Based on the success with reduced form factors, this was expected (36) to hold for $-\hat{t}_p$ and $-\hat{t}_n$ larger than 1 GeV^2. In terms of photon lab energy $E_\gamma^{\rm Lab}$ and the center-of-mass angle θ_{cm} for the proton, these constraints imply

$$\frac{1}{2} M_d E_\gamma^{\rm Lab} \left[1 - \sqrt{\frac{2E_\gamma^{\rm Lab}}{M_d + 2E_\gamma^{\rm Lab}}} |\cos\theta_{cm}|\right] \geq 1\,\text{GeV}^2\,. \qquad 55.$$

The minimal energy requirement is found at 90°, where $E_\gamma^{\rm Lab} \geq 1$ GeV. For angles near 55° (or 125°) $E_\gamma^{\rm Lab}$ should be above 2 GeV; near 35° (or 145°) it should be above 3.5 GeV. The energy requirement then grows rapidly for smaller angles.

Brodsky & Hiller (36) developed a model for f, based on a simple meson disintegration analogy. The model was not found to be particularly useful because accessible momentum transfers are too small in regions near $\theta_{cm} = 0°$ and 180°.

ASYMPTOTIC MESON-EXCHANGE THEORY The asymptotic meson-exchange theory (66) is fully relativistic. For photon energies greater than 1 GeV, the distance probed in the two-nucleon system is well under 1 fm where traditional deuteron wave functions are not well constrained. The traditional approach of using an r-space relativistic deuteron wave function is abandoned in favor of an asymptotic *dNN* form factor that schematically describes the hadronic vertex at small distances. The form of the dNN form factor is similar to the three-pole asymptotic deuteron wave function used (67, 68) to describe electron-deuteron elastic scattering at high momentum transfer. This approach gives a much improved description of the deuteron photodisintegration data at high energies compared with the traditional meson-exchange approach (69, 70).

OTHER PROCESSES For electrodisintegration, the reduced amplitude is (36)

$$m \sim f\left(\frac{\text{invariants}}{s}\right) \Big/ p_T^2 \,. \qquad 56.$$

A model for f has been suggested (36), based on the lowest-order diagrams for the meson disintegration process $\gamma^* M \to q\bar{q}$ and assumption of one-photon exchange. This could serve as a model for the background to production of dibaryon resonances (71).

Brodsky (7) has considered processes that use $\bar{p}$ beams. In particular, for $\bar{p}d \to \pi p$ the reduced amplitude analysis yields

$$\frac{d\sigma}{dt} \sim \frac{f^2(\theta_{cm})}{p_T^2} F_N^2(\hat{t}) F_N^2(\hat{s}) \,, \qquad 57.$$

where $\hat{t} = (p - p_d/2)^2$ and $\hat{s} = (\bar{p} + p_d/2)^2$, with p, $\bar{p}$, and p_d, the momenta of the proton, antiproton, and deuteron, respectively. Kondratyuk & Sapozhnikov (72) analyzed data for this process and found that the magnitude of the data is not explained by traditional nuclear physics.

4.2 *Comparison with Experiment*

Two-body photodisintegration of the deuteron is one of the simplest nuclear processes. Photodisintegration is particularly effective (73) in depositing energy in the nucleus because the entire photon energy must be absorbed by the nucleus. The status of measurements of high-energy differential cross section and polarization is presented here.

DIFFERENTIAL CROSS SECTION During the past decade, measurements of the cross section for the exclusive process $\gamma d \to pn$ have been advanced from a photon energy of 1 GeV up to a photon energy of 4 GeV in a series of experiments performed at SLAC (74–76), and most recently, at the Thomas Jefferson National Accelerator Laboratory (TJNAF) (77). Surprisingly, the results, particularly at $\theta_{cm} = 90^\circ$, have followed the constituent counting rule (49). The quantity $s^{11} d\sigma/dt$ is shown as a function of the photon energy in Figure 5. A fit to these data from approximately 1 GeV to 4 GeV reveal that the results follow a $1/s^{n-2}$ dependence where $n - 2 = 11.4 \pm 0.2$.

This result is particularly surprising because one would expect the repulsive core in the nucleon-nucleon reaction to ensure that the six constituent quarks in the deuteron could not be confined to a small spatial region as required by the pQCD interpretation of the constituent counting rule. Although the reason is unclear, the data exhibit a scaling feature from a photon energy of 1–4 GeV.

The solid and dashed-dot curves in Figure 5 are the results of traditional meson-exchange calculations (69, 70) and are in reasonable agreement with

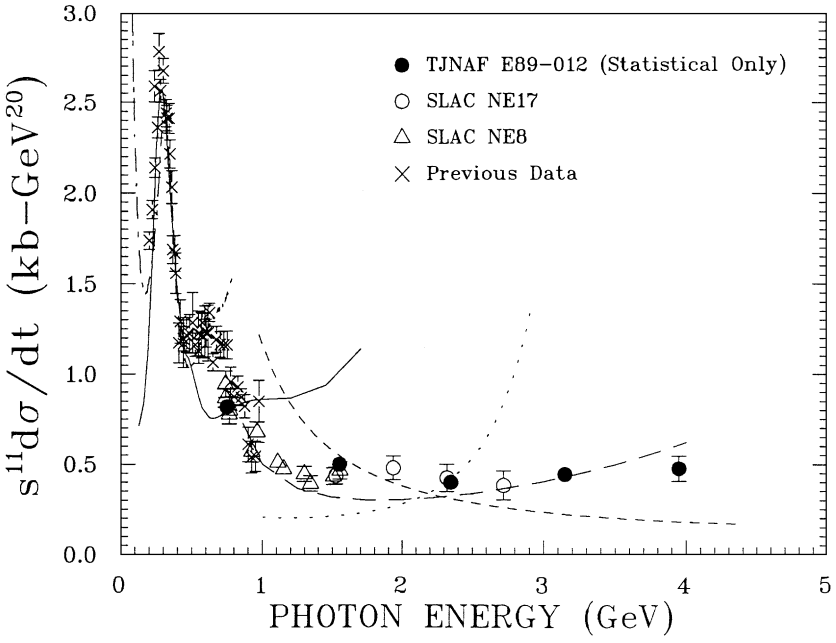

Figure 5 Summary of data as a function of photon energy at $\theta_{cm} = 90^\circ$. The solid circles are the preliminary TJNAF data with statistical uncertainties only. The curves are explained in the text.

the data (78) below 0.5 GeV. The asymptotic meson-exchange calculation, arbitrarily normalized at 1 GeV, is shown as the long-dashed line in the Figure and is in fair agreement with the data. The dashed curve is the result of the RNA where the curve was arbitrarily normalized at 0.8 GeV. Again, it is surprising that the constituent counting rule appears to describe the energy dependence of the cross section much better than the RNA, which is expected to describe intermediate energy data as discussed in Section 4.1. The quark-gluon string approach (79), the dotted curve, considers only the t-channel in the same fashion as Regge theory. Thus this calculation is not expected to describe the $\theta_{cm} = 90^\circ$ data.

If indeed, there is a transition to the scaling regime which occurs at a photon energy of 1 GeV, then it is essential to determine the value of the transition to scaling at other reaction angles. The transition value will determine which kinematical variable leads to scaling and will greatly advance our understanding of the underlying dynamics. Unfortunately, the data are not of sufficient quality to exhibit conclusively this same scaling feature at other angles. For example, at $\theta_{cm} = 37^\circ$, it appears that the data have an approximately $1/s^{10}$ dependence.

The reason for this is that photon energy is not the relevant parameter, but rather the transverse momentum, p_T, may be the correct scaling variable (36). The values of p_T are relatively low at 37°, and a photon energy of more than 3 GeV would be necessary to achieve a p_T per nucleon greater than 1 GeV/c. Clearly, more data are needed at higher energy at the smaller angles to test for scaling. Plans (80) are under way to extend these measurements up to a photon energy of 5.5 GeV at TJNAF.

POLARIZATION Another feature of constituent scaling is that vector polarizations should vanish (24) in the scaling region. This effect arises from the fact that at small transverse sizes in the deuteron orbital angular momenta become small so that the hadron helicity is just given by the quark helicities. Since quark helicities are conserved in the single-gluon exchange process, the hadron helicity should be conserved. This leads to the absence of hadron helicity flip amplitudes, which are necessary for a nonvanishing vector polarization.

There have been a number of searches for hadron helicity conservation in high-energy proton-proton (pp) scattering. However, there is no evidence (81) that vector polarizations vanish at high energies in this process. A possible explanation (82, 83) for the results seen in pp scattering is that the Landshoff amplitude interferes with the hard scattering amplitude to give the vector polarization. Indeed, plausible models for the interfering Landshoff and short-distance amplitudes lead to results that match the existing pp polarization data fairly well (see Figure 6). The Landshoff terms, or long-distance quark-quark scattering terms, are ubiquitous in hadron-hadron interactions, but absent in photoreactions because the incident photon couples with only one quark in the target hadron – whereas an incident hadron could couple with more than one quark in the target. Unfortunately, no experiments such as $\gamma d \rightarrow \vec{p}n$ have been performed above a photon energy of 1 GeV at $\theta_{cm} = 90°$, although plans (84) are under way to perform such measurements.

4.3 *Tensor Polarization for Deuteron-Proton Elastic Scattering*

Deuteron-proton (dp) elastic scattering has been carried out at high momentum transfer. (One names the deuteron first because the deuteron is often the projectile with the proton target at rest in the lab.) Of particular interest is the tensor analyzing power T_{20} for scattering backward in the center of mass. Data (85) is shown in Figure 7. The horizontal axis is t, which is defined by

$$t = (d - d')^2, \qquad 58.$$

where d and d' are the momenta of the incoming and outgoing deuterons. Note that t is precisely the same as the momentum transfer q^2 in the elastic ed case.

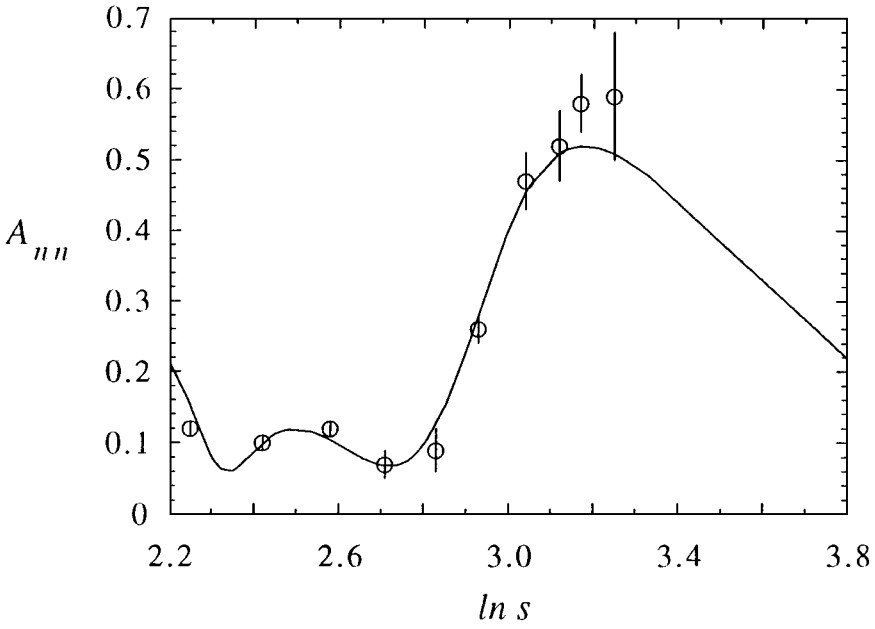

Figure 6 The beam-target spin correlation A_{nn} at 90° c. m. for *pp* elastic scattering as a function of $\ln s$ (with s in GeV^2), based on Reference 82.

Note also that the values of $|t|$ are very high compared to what can be reached in the electromagnetic case.

The theoretical curves shown (85) are based on the standard neutron-proton model of the deuteron, being a one-neutron exchange model or impulse approximation that uses the Paris and Bonn wave functions, made using the light-front techniques outlined in Sections 2.2 and 2.3. This is the simplest relativistic calculation possible in a hadronic view of the deuteron and, in this sense, is the analog of the relativistic impulse approximation calculations of *ed* elastic scattering. The overall results for T_{20} in the dp and *ed* cases are visually similar, although the details of the calculations are quite different, and the crossing of the $T_{20} = 0$ axis is at different values of t or q^2. The data for T_{20} in the dp case does not agree well with the impulse approximation using the standard wave functions. In particular, although the data start out negative, in concert with the calculations, they never cross the axis to go positive although measurements exist at values of t well beyond where the theory crosses. It will be interesting to see what happens in the *ed* case when higher Q^2 data are available.

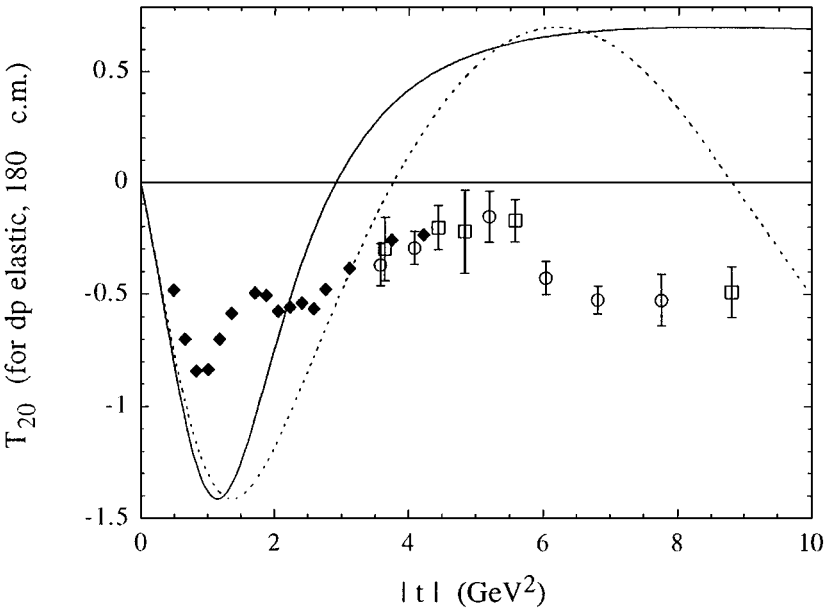

Figure 7 Tensor analyzing power T_{20} for deuteron-proton (dp) elastic scattering. The data are from Saclay and Dubna. This figure is based on one in Reference 85; only the total errors are shown. The solid line and dotted lines show the predictions of the Paris and Bonn wave functions in a one-neutron exchange model.

It is, of course, the tail of the wave function that matters for high momentum transfer reactions, and a suggestion made by Kobushkin (86) using six-quark cluster ideas will be mentioned here. If there is a six-quark cluster in the deuteron, it, rather than some meson-exchange potential, will need to be considered since the tail depends on short range in momentum space. Grouping quarks into sets of three, the cluster is a superposition of colored and colorless quark triplets (the latter, if isospin 1/2, being putative neutrons and protons that can come out into one's detector), and considering one-gluon exchanges between the sets, Kobushkin makes a prediction for the D/S ratio at high relative neutron-proton momenta. This leads to

$$T_{20} = \frac{-7}{17\sqrt{2}} \approx -0.3 \qquad 59.$$

which is in the ballpark of the data. (There is also a prediction that κ – the polarization transfer from a vector polarized initial deuteron to the final proton – will be $+18/17$. At the highest momentum transfer where there is data ($|t| \approx 4$ GeV^2), the standard wave functions predict about -0.7. The data

gives roughly -0.2 ± 0.1 (87), an uncertainty small enough to exclude either prediction.

5. MOMENTS

5.1 *General Results for Spin-1 Composites*

At zero momentum transfer, the deuteron form factors are proportional to the usual static quantities of charge e, magnetic moment μ_d, and quadrupole moment Q_d:

$$eG_C0 = e\,, \quad eG_M0 = 2M\mu_d\,, \quad eG_Q0 = M^2Q_d\,. \tag{60.}$$

Obtaining the magnetic and quadrupole moments by summing moments of constituents is correct only when mass M of the composite is much larger than the masses m_i of the constituents, and the radius R of the composite is much larger than the Compton scale $1/M$. Only then are the dynamical contributions $\mathcal{O}(e/m_i)$, $\mathcal{O}(eR)$, and $\mathcal{O}(eR^2)$ large compared to kinematical boost effects (37).

In the limit of zero radius, the magnetic and quadrupole moments of a spin-1 system approach the canonical values of e/M and $-e/M^2$, respectively (27). This can be seen from the following sum rules (88–90) for anomalous moments $\mu_a \equiv \mu_d - e/M$ and $Q_a \equiv Q_d + e/M^2$:

$$\mu_a^2 = \frac{1}{\pi}\int_{\omega_{\rm th}}^{\infty}\frac{d\omega}{\omega}\left[\sigma_P(\omega) - \sigma_A(\omega)\right]\,, \tag{61.}$$

where σ_P (σ_A) is the total cross section for absorption of a photon with spin parallel (antiparallel) to the spin of the target, ω is the photon energy, and $\omega_{\rm th}$ is the excitation threshold, and

$$\mu_a^2 + \frac{2t}{M^2}\left(\mu_a + \frac{M}{2}Q_a\right)^2 = \frac{1}{4\pi}\int_{\nu_{\rm th}^2}^{\infty}\frac{d\nu^2}{(\nu - t/4)^3}\left(\mathcal{I}m\ f_P(s,t) - \mathcal{I}m\ f_A(s,t)\right)\,, \tag{62.}$$

with f_P (f_A) the helicity amplitude for parallel (antiparallel) spins, $\nu = (s-u)/4$, and $\nu_{\rm th}$ the threshold. The first sum rule is the spin-1 extension (89) of the Drell-Hearn-Gerasimov (88) sum rule. The second follows from work of Tung (90). In the case of the quadrupole moment, there is no sum rule related to total cross sections, and nonforward amplitudes must be used. Because the zero-radius limit implies infinite excitation threshold, the anomalous moments are forced to be zero (27).

This zero result implies that a D wave is not required for a spin-1 composite to have a nonzero quadrupole moment (27). Model calculations by Schlumpf

& Brodsky (37) yield $Q_d/e = -0.0036\,\mathrm{GeV}^{-2}$ for a pure S-wave state. The origin of such effects is found in corrections to interactions due to Wigner boosts (91, 92) that survive in the static limit.

5.2 *Light-Front Models*

Schlumpf has developed light-front models for two- and three-body bound states in which the wave function is a product of a momentum-space wave function and a spin-isospin wave function. The latter is found by symmetry requirements (93). An eigenfunction of J^2 and J_z is formed in the rest frame by applying a Melosh rotation (92) to the spinors. Only the S-wave component is considered.

The momentum-space wave function is taken to be a model function

$$\psi(\mathcal{M}^2) = N \exp(-\mathcal{M}^2/2\beta^2) \qquad 63.$$

of the invariant mass $\mathcal{M}^2 = \sum_i (k_{i\perp}^2 + m_N^2)/x_i^2$. The results are found to be insensitive to the precise form of the wave function (94). A value of 0.12 GeV for β closely matches the S-state wave function used in Reference 95.

From the model, the moments μ_d and Q_d are computed as functions of the charge radius R defined by $R^2 = -6F'0$, where $F(Q^2) = G_{++}^+(Q^2)$. A range of R values can be considered by varying β. For fixed nucleon and deuteron mass, the limit $\beta \to 0$ yields $R = \infty$ and

$$\mu_d = \mu_p + \mu_n + \frac{2m_N - M_d}{M_d}\mu_N\,, \qquad 64.$$

with μ_p and μ_n the nuclear moments and μ_N the nuclear magnetron. Thus the correction to the usual nonrelativistic result is of order ϵ_d/M_d, the fractional binding energy. The same result was obtained by Chung et al (46), and the correction term is among the relativistic corrections obtained by Kondratyuk & Strikman (96). In the same infinite-radius limit the quadrupole moment becomes

$$\frac{Q_d}{e} = \frac{M_d - 2m_N}{2M_d m_N^2}(1 + a_p + a_n)\,, \qquad 65.$$

where $a_{p(n)}$ is $(\mu_{p(n)} - e/2m_{p(n)})\,2m_{p(n)}/e$, the dimensionless anomalous moment of the proton (neutron). The zero-radius ($\beta = \infty$) limit of the model reproduces the correct results for a point-like spin-1 object: The anomalous moments become zero.

The model interpolates smoothly between the limits. The value of -0.0036 GeV^{-2} quoted earlier is found at the value of β that yields the physical deuteron radius.

6. SUMMARY AND OUTLOOK

The application of perturbative QCD to the deuteron has produced a number of interesting results. They include dimensional scaling (18) for cross sections (26) and elastic form factors (28), short-distance dominance of non-nucleonic components (17), and predictions for the form factor ratio B/A and the tensor analyzing power T_{20} (27).

Careful attention to momentum scales is important. For the dominant form factor, data (21, 22) implies that scaling begins at $Q^2 \sim 1\,\mathrm{GeV}^2$. However, a direct calculation by summing quark-gluon diagrams linking nucleons (48) does not obtain the requisite normalization. This discrepancy may be due to non-nucleonic contributions (48), incorrect momentum scales in the running coupling (5), or strictly nonperturbative (soft) contributions (97).

For the subdominant form factors, there are two important Q^2 scales (27), $2\Lambda_{\mathrm{QCD}}M_d$ and $4M_d^2$. Between them the subdominant form factors should be considered (28), unless one works only to leading order in $\Lambda_{\mathrm{QCD}}/M_d$ (27). Above $4M_d^2$ they can be neglected. The range of energy and momentum transfer necessary to check these results is close to being available.

Inclusion of nonperturbative corrections via reduced-amplitude analysis (20, 36, 51) has reduced the threshold for appearance of scaling. It has been less successful for photodisintegration at 90° (74–77) where simple dimensional counting rules give better results; data at other angles and higher photon energies are needed to fully explore the prediction.

Model calculations of current matrix elements have encountered difficulties related to violations of rotational covariance (31–33). Ways to surmount these difficulties have been put forward (34, 60). The pQCD results are on a stronger footing because the angular condition (41) is consistent with the predicted asymptotic behavior of form factors (33).

Analysis of the static properties of the deuteron can also benefit from the relativistic point of view adopted when working with pQCD. Extension of the model by Schlumpf & Brodsky (37) to include D-wave components may provide a more consistent phenomenology.

With the arrival of the Thomas Jefferson National Accelerator Facility the outlook for extending the measurements to higher momentum and energy transfer for electron-deuteron scattering and photodisintegration is exceedingly bright. For electron-deuteron elastic scattering, the quantities $A(Q^2)$, $B(Q^2)$, and t_{20} are already proposed for new measurements at TJNAF. Plans exist to extend cross-section measurements for photodisintegration of the deuteron up to 5.5 GeV. In addition, the photoproton polarization experiments at TJNAF should provide the first information on the issue of hadron helicity conservation in photoreactions. The $d(e,e'N)$ experiments at TJNAF and the $d(p,2p)$ experiments

at high missing momentum at IUCF should provide additional constraints on the short-range behavior of the deuteron wave function.

ACKNOWLEDGMENTS

We have benefited from discussions and help from more colleagues than we can easily name, and we thank them all. CEC thanks the NSF for support under grant PHY-9600415 and RJH thanks the NSF for support under grant PHY-9420787.

Literature Cited

1. For general reviews of quantum chromodynamics, see Collins JC, Soper DE. *Annu. Rev. Nucl. Part. Sci.* 37:383 (1987); Reya E. *Phys. Rep.* 69:195 (1981)
2. Gross DJ, Wilczek F. *Phys. Rev. Lett.* 30:1343 (1973); Politzer H. *Phys. Rev. Lett.* 30:1346 (1973)
3. Brodsky SJ, Lepage, GP. In *Perturbative Quantum Chromodynamics*, ed. AH Mueller, pp. 93-240. Singapore: World Sci. (1989)
4. Lepage GP, Brodsky SJ. *Phys. Rev.* D22:2157-98 (1980); *Phys. Lett.* 87B:359 (1979); *Phys. Rev. Lett.* 43:545 (1979); 43:1625(E) (1979)
5. Brodsky SJ. *Proc. Orbis Scientiae 1996* (1996).
6. Brodsky SJ, Lu HJ. *Proc. PASCOS 95*, Johns Hopkins Univ. (1995)
7. Brodsky SJ, Schlumpf F. *Prog. Part. Nucl. Phys.* 34:69-86 (1995)
8. Brodsky SJ, Ji CR. *Quarks and Leptons*, ed. CA Engelbrecht. Lecture Notes in Physics 248. Berlin: Springer-Verlag. (1986)
9. Carlson, CE. *New Vistas in Electro-Nuclear Physics*, Proceedings of a NATO Advanced Study Institute in Banff, Canada, August 1985, ed. E. L. Tomusiak, H. S. Kaplan, and E. T. Dressler, p. 101. New York: Plenum (1986)
10. Frankfurt LL, Strikman MI. *Phys. Rep.* 76:215-347 (1981)
11. Frankfurt LL, Strikman MI. *Phys. Rep.* 160:235-427 (1988)
12. Dirac PAM. *Rev. Mod. Phys.* 21:392 (1949)
13. For reviews and discussion, see Brodsky SJ, et al. In *Springer Tracts in Modern Physics* 100. Berlin: Springer-Verlag (1982); Lepage GP, et al. In Proceedings of the 1981 Banff Summer Institute on Particle Physics, Alberta, Canada; Namyslowski JM. *Prog. Part. Nucl. Phys.* 14:49 (1985); Brodsky SJ, Pauli HC. In *Recent Aspects of Quantum Fields*, ed. H Mitter, H Gausterer. Lecture Notes in Physics 396. Berlin: Springer-Verlag (1991); Brodsky SJ, et al. *Part. World* 3:109 (1993); Burkardt M. *Adv. Nucl. Phys.* 23:1 (1996)
14. Wilson KG, et al. *Phys. Rev.* D49:6720 (1994)
15. Matveev V, Sorba P. *Nuovo Cim.* 45A: 257 (1978); Kobyshikin AP (Kobushkin in newer works by the same author). *Yad. Fiz.* 28:495 (1978) [*Sov. J. Nucl. Phys.* 28:252 (1978)]
16. Harvey M. *Nucl. Phys.* A352:301 (1981); A352:326 (1981)
17. Brodsky SJ, Ji CR. *Phys. Rev.* D33:1406-14 (1986)
18. Brodsky SJ, Farrar GR. *Phys. Rev.* D11:1309-30 (1975); *Phys. Rev. Lett.* 31:1153 (1973); see also Matveev VA, et al. *Lett. Nuovo Cim.* 7:719 (1973)
19. Brodsky SJ, et al. *Phys. Rev. Lett.* 51:83-86 (1983)
20. Brodsky SJ, Chertok BT. *Phys. Rev.* D14:3003-20 (1976); *Phys. Rev. Lett.* 37:269-72 (1976)
21. Arnold RG, et al. *Phys. Rev. Lett.* 35:776-79 (1975); Arnold RG. private communication
22. Cramer R, et al. *Z. Phys.* C29:513-18 (1985); Platchkov S, et al. *Nucl. Phys.* A510:740-58 (1990)
23. Arnold RG, et al. *Phys. Rev.* C21:1426 (1980); Glaser V, Jaksic B. *Nuovo Cim.* 5:1197 (1957); Gourdin M. *Nuovo Cim.* 28:533 (1963)

24. Brodsky SJ, Lepage GP. *Phys. Rev.* D24:2848 (1981)
25. Carlson CE, Gross F. *Phys. Rev. Lett.* 53:127-29 (1984)
26. Coester F. In *Proceedings of the International Conference on Medium and High-Energy Nuclear Physics*, ed. WYP Hwang, KF Liu, Y Tzeng, pp. Singapore: World Sci. (1988)
27. Brodsky SJ, Hiller JR. *Phys. Rev.* D46:2141-49 (1992)
28. Kobushkin A, Syamtomov A. *Phys. Rev.* D49:1637 (1994)
29. Carlson CE. *Nucl. Phys.* A508:481c (1990)
30. Ferro-Luzzi M, et al. *Phys. Rev. Lett.* 77:2630 (1996); Popov SG, et al. In *Proceedings of the 8th International Symposium on Polarization Phenomena in Nuclear Physics*, ed. EJ Stephenson, SE Vigdor. AIP Conf. Proc. 339:530 (1995); Garcon M, et al. *Phys. Rev.* C49:2516-37 (1994); The I, et al. *Phys. Rev. Lett.* 67:173-76 (1991); Boden B, et al. *Z. Phys.* C49:175 (1991); Gilman R, et al. *Phys. Rev. Lett.* 65:1733-36 (1990); Voitsekhovshii BB, et al. *Pis'ma Zh. Eksp. Teor. Fiz.* 43:567-69 (1986) [*JETP Lett.* 43:733-36 (1986)]; Dmitriev VM, et al. *Phys. Lett.* 157B:143-45 (1985); Schulze ME, et al. *Phys. Rev. Lett.* 52:597-600 (1984)
31. Gell-Mann M. In *Strong and Weak Interactions: Present Problems*, ed. A Zichichi. New York: Academic (1966); Osborn H. *Nucl. Phys.* B38:429 (1972); Leutwyler H, Stern J. *Ann. Phys.* 112:94 (1978)
32. Grach IL, Kondratyuk LA. *Sov. J. Nucl. Phys.* 39:198 (1984)
33. Keister BD. *Phys. Rev.* D49:1500 (1994)
34. Karmonov VA. On ambiguities of the spin-1 electromagnetic form factors in light-front dynamics. Submitted to *Nucl. Phys.* A (1996)
35. Karmanov VA, Smirnov AV. *Nucl. Phys.* A546:691 (1992); A575:520-48 (1994)
36. Brodsky SJ, Hiller JR. *Phys. Rev.* C28:475-82 (1983); C30:412(E) (1984)
37. Schlumpf F, Brodsky SJ. *Phys. Lett.* B360:1-6 (1995)
38. Appelquist R, Primack JR. *Phys. Rev.* D1:1144 (1970)
39. For a review of the light-front formalism as applied to few-body systems, see Keister BD, Polyzou WN. *Adv. Nucl. Phys.* 20:225 (1991)
40. Coester F. *Prog. Part. Nucl. Phys.* 29:1 (1992)
41. For a number of papers on renormalization and other issues for light-front QCD, see *Theory of Hadrons and Light-Front QCD*, ed. Glazek SD. Singapore: World Sci. (1995)
42. Ableev VG, et al. *Nucl. Phys.* A393:491 (1983)
43. Bosveld GD, Diepreink AEL, Tenner AG. *Phys. Rev.* D49:2379 (1994)
44. Carlson CE, Hanlon J, Lassila KE. Experimental and theoretical results for weak charge current backward proton production. Report WM-96-103
45. Hofstadter R. *Annu. Rev. Nucl. Sci.* 7:231 (1957)
46. Chung PL, et al. *Phys. Rev.* C37:2000 (1988)
47. Drell SD, Yan TM. *Phys. Rev. Lett.* 24:181 (1970)
48. Farrar GR, et al. *Phys. Rev. Lett.* 74:650-53 (1995)
49. Ji CR, Brodsky SJ. *Phys. Rev.* D34:1460-73 (1986)
50. Brodsky SJ, Ji CR. *Phys. Rev.* D33:2653-59 (1986)
51. See, for example, Gurvitz SA. *Phys. Rev.* C22:1650 (1980)
52. Kisslinger LS. *Phys. Lett.* B112:307 (1982); Cheng TS, Kisslinger LS. *Nucl. Phys.* A457:602 (1986); *Phys. Rev.* C35: 1432 (1987); Lu LC, Cheng TS. *Phys. Lett.* B386:69-74 (1996)
53. González P, Vento V. *Few-Body Syst.* 2:145 (1987)
54. Gross F, Buck W. Private communication
55. Dijk H, Bakker BLG. *Nucl. Phys.* A494:438 (1989)
56. Carlson CE, Lassila KE, Sukhatme UP. *Phys. Lett.* 263: 277 (1991); Carlson CE, Lassila KE. *Phys. Lett.* 317B: 205 (1993); Carlson CE, Lassila KE. *Phys. Rev.* D51: 364 (1995)
57. CEBAF experiment E-94-102, Electron scattering from a high momentum nucleon in deuterium. Kuhn SE and Griffioen KA, spokesmen.
58. Lev FM. *Ann. Phys.* 237:355-419 (1995)
59. Cardarelli F, et al. *Phys. Lett.* B349:393-399 (1995)
60. Fuda MG. *Ann. Phys.* 197:265 (1990); 231:1-40 (1994)
61. Haftel MI, et al. *Phys. Rev.* C22:1285 (1980)
62. Dymarz F, Khanna FC. *Phys. Rev. Lett.* 56:1448 (1986)
63. Auffret S, et al. *Phys. Rev. Lett.* 54:649-52 (1985); Arnold RG, et al. *Phys. Rev. Lett.* 58:1723-26 (1987); Bosted PE, et al. *Phys. Rev.* C42:38 (1990)
64. Van Orden JW, et al. *Phys. Rev. Lett.* 75:4369 (1995); Schiavilla R, Riska DO. *Phys. Rev.* C43:437 (1991); Blunden PG.

Phys. Rev. C40:1541 (1989); Hummel E, Tjon JA. *Phys. Rev. Lett.* 63:1788 (1989)
65. Beise E, Kox S, et al. TJNAF proposal E94-018 (1994); Petratos GG, et al. TJNAF proposal E91-026 (1994)
66. Nagornyi SI, et al. *Sov. J. Nucl. Phys.* 55:189 (1992)
67. Buck WW, Gross F. *Phys. Rev.* D20:2361 (1979)
68. Gross F, Keister BD. *Phys. Rev.* C28:823 (1983)
69. Lee T-SH. Argonne Natl. Lab. Rep. No. PHY-5253-TH-88; In *Proceedings of the International Conference on Medium and High Energy Nuclear Physics*, Taipai, Taiwan, 1988, p. 563. Singapore:World Sci. (1988)
70. Laget JM. *Nucl. Phys.* A312:265 (1978)
71. Lichtenberg DB, et al. Invited talk at International Workshop on Diquarks, Turin, Italy, 1996 hep-ph/9611429; Jaffe RL. *Phys. Rev. Lett.* 38:195 (1977); for recent possible evidence, see Brodowski W, et al. *Z. Phys.* A355:5 (1996); Pickarz H. In *Intersections Between Particle and Nuclear Physics*, AIP Conf. Proc. 243, ed. WTH Van Oers. New York: AIP (1992); for a review of diquarks that contains discussion and references for dibaryons, see Anselmino M, et al. *Rev. Mod. Phys.* 65:1199 (1993)
72. Kondratyuk LA, Sapozhnikov MG. *Phys. Lett.* B220:333 (1989)
73. Holt RJ. *Phys. Rev.* C41:2400 (1990)
74. Napolitano J, et al. *Phys. Rev. Lett.* 61:2530 (1988)
75. Freedman SJ, et al. *Phys. Rev.* C48:1864 (1993)
76. Belz JE, et al. *Phys. Rev. Lett.* 74:646 (1995)
77. Abbott D, et al. Proc. Particle and Nuclear Int. Conference, Williamsburg, VA, May, 1996; Proc. of Int. Workshop on Electron Scattering from Nuclei, Elba, July, 1996
78. Dougan P, et al. *Z. Phys* A276:55 (1976); Ching R, Schaef C. *Phys. Rev.* 141:1320 (1966); Myers H, et al. *Phys. Rev* 121:630 (1961); Arends J, et al. *Nucl. Phys.* A412:509 (1984)
79. Kondratyuk LA, et al. *Phys. Rev.* C48:2491 (1993)
80. Holt R, et al. TJNAF proposal E96-003 (1996)
81. Crabb DG, et al. *Phys. Rev. Lett.* 65:3241 (1990)
82. Carlson CE, et al. *Phys. Rev.* D 46:2891 (1992)
83. Ramsay G, Sivers D. *Phys. Rev.* D 45:79 (1992)
84. Gilman R, et al. TJNAF proposal E89-019 (1989)
85. Azhgirey LS, et al. *Phys. Lett.* 391B:22 (1997)
86. Kobushkin AP. *J. Phys.* G19:1993 (1993)
87. Punjabi V, et al. *Phys. Lett.* 350B:178 (1995)
88. Drell SD, Hearn AC. *Phys. Rev. Lett.* 16:908 (1966); Gerasimov SB. *Sov. J. Nucl. Phys.* 2:430-433 (1966)
89. Hosoda M, Yamamoto K. *Prog. Theor. Phys.* 36:426-27 (1966); see also Brodsky SJ, Primack JR. *Ann. Phys.* 52:315 (1969)
90. Tung WK. *Phys. Rev.* 176:2127 (1968); Bardeen WA, Tung WK. *Phys. Rev.* 173:1423 (1968)
91. Wigner E. *Ann. Math.* 40:149 (1939)
92. Melosh HJ. *Phys. Rev.* D9:1095 (1974); Kondratyuk LA, Ternet'ev MV. *Sov. J. Nucl. Phys.* 31:561 (1980)
93. Schlumpf F. *Phys. Rev.* D47:4114-21 (1993); D49:6246(E) (1994)
94. Brodsky SJ, Schlumpf F. *Phys. Lett.* B329:111 (1994)
95. Machleidt R, et al. *Phys. Rep.* 149:1 (1987)
96. Kondratyuk LA, Strikman MI. *Sov. J. Nucl. Phys.* 37:794 (1983)
97. Isgur N, Llewellyn-Smith CH. *Nucl. Phys.* B317:526 (1989)
98. Lassila KE, Sukhatme UP. *Phys. Lett.* 209B:343 (1988)
99. Anderson RL, et al. *Phys. Rev.* D14:679 (1976)
100. White G, et al. *Phys. Rev.* D49:58 (1994)
101. Matthews JL, Owens RO. 1111571973.
102. Belz JE. Ph.D. thesis, California Institute of Technology, 1994 (unpublished)
103. CEBAF proposal 94-012, R. Gilman, R. Holt (spokespersons)

Annual Review of Nuclear and Particle Science
Volume 47, 1997

CONTENTS